Improved cosmological constraints on axion-lepton interactions

Marcin Badziak, Adam Gomułka, Maxim Laletin and Krzysztof Szafrański

Institute of Theoretical Physics, Faculty of Physics, University of Warsaw, ul. Pasteura 5, PL-02-093 Warsaw, Poland

E-mail: Marcin.Badziak@fuw.edu.pl, Adam.Gomulka@fuw.edu.pl, Maxim.Laletin@fuw.edu.pl, Krzysztof.Szafranski@fuw.edu.pl

Abstract: We present updated cosmological constraints on axion-lepton interactions based on state-of-the-art computations of the thermal axion abundance. By combining Planck Cosmic Microwave Background (CMB) data with baryon acoustic oscillation (BAO) measurements from DESI DR2, we derive improved limits on both lepton-flavor-conserving (LFC) and lepton-flavor-violating (LFV) axion couplings. Incorporating finite axion mass effects substantially strengthens the bounds for axion masses above 0.1 eV compared to those inferred from the $\Delta N_{\rm eff}$ constraint alone. The bounds on the LFC axion-tau coupling and LFV axion couplings to tau and muon or electron are improved by several orders of magnitude and the lower bound on the axion decay constant may exceed 10⁶ and 10⁸ GeV, respectively, for axion masses above 1 eV. Our cosmological constraints on LFC axion couplings to muons and taus and LFV axion couplings to tau and muon or electron are stronger than all other constraints for masses above 0.3 eV. In particular, they are stronger than recent collider constraints from Belle-II on $\tau \to la$ decays, where l = e or μ . The collider constraints on $\mu \to ea$ decays are weaker than the cosmological constraints for axion masses above 100 eV. Our results are relevant for both the QCD axion and axion-like particles (ALPs).

Co	ontents				
1	Introduction				
2	2 Thermal production of axions				
3 Cosmological analysis methodology					
4	Results 4.1 Lepton-flavor conserving (LFC) interactions	8 8			
	4.2 Lepton-flavor violating (LFV) interactions 4.3 Warm DM constraint	11 13			
5	Conclusions	15			
\mathbf{A}	Implementation of axion distribution functions in CLASS	17			
В	B Results of full scans with varying axion mass				
\mathbf{C}	CMB power spectrum and matter power spectrum for τ decays	20			

1 Introduction

Pseudo-Nambu-Goldstone bosons (PNGB) arising from spontaneously broken approximate global symmetries appear in many well-motivated extensions of the Standard Model (SM). A particularly well-motivated PNGB is the QCD axion which arises from spontaneously broken Peccei-Quinn (PQ) symmetry which is introduced to solve the strong CP problem [1]. The QCD axion is a good dark matter (DM) candidate [2–4] and can be linked to a mechanism responsible for the observed baryon asymmetry of the Universe [5]. PQ symmetry is broken only by non-perturbative QCD effects leading to a small but non-zero axion mass which is entirely determined by the axion decay constant f [6]:

$$m_a \approx 0.569(51) \left(\frac{10^7 \text{ GeV}}{f}\right) \text{ eV}.$$
 (1.1)

In QCD axion models there is a lower bound on f stemming from astrophysical constraints. In minimal QCD axion models, such as KSVZ [7, 8] or DFSZ [9, 10] models, the lower bound on the QCD axion decay constant is at the level of few times 10^8 GeV which translates to the QCD axion mass of order $\mathcal{O}(0.01)$ eV [11, 12]. In the so-called astrophobic axion models [13–19] this bound can be relaxed and a value of f even as small as few times 10^6 GeV [18] may be allowed leading to the QCD axion mass $\mathcal{O}(1)$ eV. One should, however, keep in mind

that the astrophysical constraints rely on phenomenological models of stars which are not fully understood, thus, they suffer from large theoretical uncertainties.

The above mentioned astrophysical bounds and the axion mass prediction (1.1) are specific for the QCD axion. For general PNGB, also known as axion-like particle, that we refer to simply as axion, f and m_a are independent parameters and, in particular, the axion mass can span many orders of magnitude and can exceed eV.

Axions are very good candidates for cold dark matter (CDM) since they are produced via the misalignment mechanism [2–4, 20] or decay of topological defects [21–24]. However, axions can be also produced thermally via interactions with SM particles in the early Universe plasma. In particular, thermally produced axions can play the role of the observed DM [25–27] provided that their lifetime is long enough and their mass is above the warm dark matter (wDM) bound from Ly- α forests [28], which have been shown to be $\mathcal{O}(10)$ keV for axions [27, 29–32].

For smaller masses, axions are not cold enough to explain all the observed DM, but may leave imprints in various cosmological observables, so the cosmological data allow to set constraints on the axion decay constant which are more robust than the astrophysical ones. Most studies so far have focused on very light, ultra-relativistic axions which contribute to dark radiation and increase the additional effective number of neutrinos $\Delta N_{\rm eff}$, which is constrained by the Big Bang Nucleosynthesis (BBN) and the Cosmic Microwave Background (CMB). In particular, the Planck satellite measurements of CMB anisotropies set an upper bound on $\Delta N_{\rm eff} \lesssim 0.3$ at 95% confidence level (C.L.) [33] which leads to an upper bound on axion couplings. There have been numerous papers devoted to the computation of axion contribution to $\Delta N_{\rm eff}$, see e.g. Refs. [19, 34–52]. The majority of works computed $\Delta N_{\rm eff}$ using instantaneous decoupling approximation or by solving Boltzmann equations for the axion number density assuming that they are in thermal equilibrium. It was recently realised that in order to obtain precise predictions for $\Delta N_{\rm eff}$ that fully exploits the expected sensitivity of planned CMB experiments, such as Simons Observatory [53], one has to relax the assumption of thermal distribution functions and solve Boltzmann equations for the actual distribution function. This improved approach was used to set constraints on the KSVZ model of the QCD axion [47, 48] and model-independent constraints on axion couplings to SM fermions [51, 52].

It is important to emphasize, however, that CMB constraints on $\Delta N_{\rm eff}$ can be used to obtain reliable constraints on axion couplings only for axion masses below $\mathcal{O}(0.1)$ eV. For larger masses axions are no longer ultra-relativistic during recombination and a dedicated cosmological analysis is required to derive constraints on axion couplings. Since the axion mass gives additional contribution to the axion energy density during and after recombination the constraints for massive axions are generically stronger than those derived solely from $\Delta N_{\rm eff}$. This have been explicitly shown for DFSZ [40, 54] and KSVZ [47, 48, 54] models for the QCD axion. To the best of our knowledge, model-independent cosmological constraints including axion mass have been derived only for the axion-photon and axion-gluon couplings [55] (but with the axion energy density obtained under instantaneous decoupling approximation).

The main objective of the present paper is to derive model-independent cosmological

constraints on axion couplings to leptons for a large range of axion masses including those larger than the recombination temperature. Constraints on axion-lepton couplings have been studied before using $\Delta N_{\rm eff}$ in Ref. [41], but as emphasised above, they underestimate constraints for axion masses above $\mathcal{O}(0.1)$ eV. We use CMB data from Planck [56, 57] and Baryon Acoustic Oscillation (BAO) data from the DESI DR2 release [58]. We consider both flavor-conserving and flavor-violating axion couplings. There are two other important improvements in our analysis that make the derived constraints more robust than those in the existing literature. First: we use the state-of-the-art computations of thermal axion abundance based on solving full Boltzmann equations for the momentum distribution functions, as recently done in Ref. [51]. This allows for a precise determination of axion energy density both in the case of axions in thermal equilibrium and in the case of axions produced via freeze-in [59]. Second: we perform a full cosmological analysis with these correct non-thermal axion distributions, instead of relying on a point-estimate to set our constraints.

We demonstrate that the effect of axion mass is very significant and may improve the constraints on axion couplings even by several orders of magnitude. In particular, we show that for axion masses above $\mathcal{O}(0.1)$ eV cosmology provides the most stringent constraints on axion couplings to muons and taus as well as on flavor-violating axion couplings to τe and $\tau \mu$.

The rest of the article is organized as follows. In Section 2 we describe the methodology behind the computation of the thermal axion abundance and show the results for axion energy density for various production channels induced by axion-lepton interactions. In Section 3 we introduce the methodology of our cosmological analysis. In Section 4 we demonstrate and analyze the resulting constraints on the axion-lepton couplings for several fixed values of the axion mass. We conclude in Section 5. Finally, in a series of Appendices we present some technical details of our cosmological analysis as well as constraints on the axion parameter space when both axion couplings and axion mass are varied simultaneously. We also elaborate on how the existence of axions impacts the CMB temperature and matter power spectra for various axion masses.

2 Thermal production of axions

In this work we consider theories which include an axion field a and are described by the following effective Lagrangian:

$$\mathcal{L} = \mathcal{L}_{SM} + \frac{1}{2} (\partial_{\mu} a)^2 - \frac{1}{2} m_a^2 a^2 + \mathcal{L}_{int}^{(a)}, \qquad (2.1)$$

where \mathcal{L}_{SM} is the SM Lagrangian, m_a is the axion mass and $\mathcal{L}_{\text{int}}^{(a)}$ includes axion interactions with SM fields that we specify later. The axion field can be thought of as a pseudo-Nambu-Goldstone boson (PNGB) of some spontaneously broken global symmetry. The explicit breaking of a global symmetry is parameterised by the axion mass. In this work we take m_a to be a free parameter, but we will also discuss a special case of the QCD axion predicted by models that solve the strong CP problem via PQ mechanism where m_a is generated solely by non-perturbative QCD effects.

In the present work we focus on axion interactions with leptons which are given by:

$$\mathcal{L}_{\text{int}}^{(a)} = \frac{\partial_{\mu} a}{2f} \,\bar{l}_i \gamma^{\mu} \left(C_{ij}^V + C_{ij}^A \gamma_5 \right) l_j \,, \tag{2.2}$$

where f is the axion decay constant. Note that axion interactions with leptons do not necessarily conserve flavor. For further convenience we define $C_i \equiv C_{ii}^A$ and $C_{ij} \equiv \sqrt{|C_{ij}^A|^2 + |C_{ij}^V|^2}$. We will refer collectively to flavor-conserving and flavor-violating couplings as C.

In order to derive the cosmological bounds we need to know the abundance of axions produced in the SM bath. We calculate it following the same methodology as in Ref. [51], namely by solving the Boltzmann equation for the axion phase-space distribution function $f_a(x,q)$ in the expanding Friedmann–Lemaître–Robertson–Walker (FLRW) Universe

$$\tilde{H}(x) (x\partial_x - \tilde{g}q\partial_q) f_a(x,q) = \mathcal{C}[f_a],$$
 (2.3)

where x = m/T is the effective unit of cosmic time inversely related to the temperature of the SM bath (m can be arbitrary, but it is convenient to use the mass of the heaviest lepton in the reaction), q = p/T is the reduced momentum of the axion, $H = H/(1 + \tilde{g})$ is the reduced Hubble parameter with $\tilde{g} = (-1/3)(d \ln h_s/d \ln x)$ being the derivative of the effective number of entropy degrees of freedom h_s and $\mathcal{C}[f_a]$ is the collision term that accounts for the impact of all the processes involving an axion on its distribution function. The exact formulae for the collision terms and interaction rates, as well as other practical details can be found e.g. in Ref. [51]. The axion abundance is determined by the integration of $f_a(x,q)$ over the phase-space of the axion, be it the number density of axions n_a or their energy density ρ_a . As demonstrated in Ref. [51] the axion abundance computed by solving the Boltzmann equation for the number density n_a under the assumption of kinetic equilibrium can noticeably deviate from the one recovered with the use of the more general momentum-dependent Boltzmann equation for the distribution function $f_a(x,q)$. However, the benefits of the latter approach extend beyond just a more precise estimate of the axion abundance – below we discuss the importance of axion distribution function $f_a(x,q)$ for cosmological probes. Throughout the text, whenever the distinction between the two approaches to compute the axion abundance is discussed, the first will be referred to as fBE (full phase-space Boltzmann equation) and the second as nBE (number-density Boltzmann equation).

In the presence of flavor-conserving axion-lepton couplings, axions are produced through scattering processes involving leptons and photons: $l^{\pm}\gamma \to l^{\pm}a$, $l^{+}l^{-} \to \gamma a$. The corresponding scattering rates are proportional to $|C_{i}|^{2}$. For flavor-violating models, axion production is dominated by the decays of the form $l_{i}^{\pm} \to l_{j}^{\pm}a$ with the corresponding decay rates proportional to $|C_{ij}|^{2}$. Flavor-violating scatterings involving photons are subdominant [26] and can be safely neglected when deriving cosmological constraints.

Cosmological constraints for axions are often derived in terms of the effective number of additional neutrino species, which is given by the following formula for axions

$$\Delta N_{\text{eff}} = \frac{8}{7} \left(\frac{11}{4}\right)^{4/3} \frac{\rho_a}{\rho_\gamma},\tag{2.4}$$

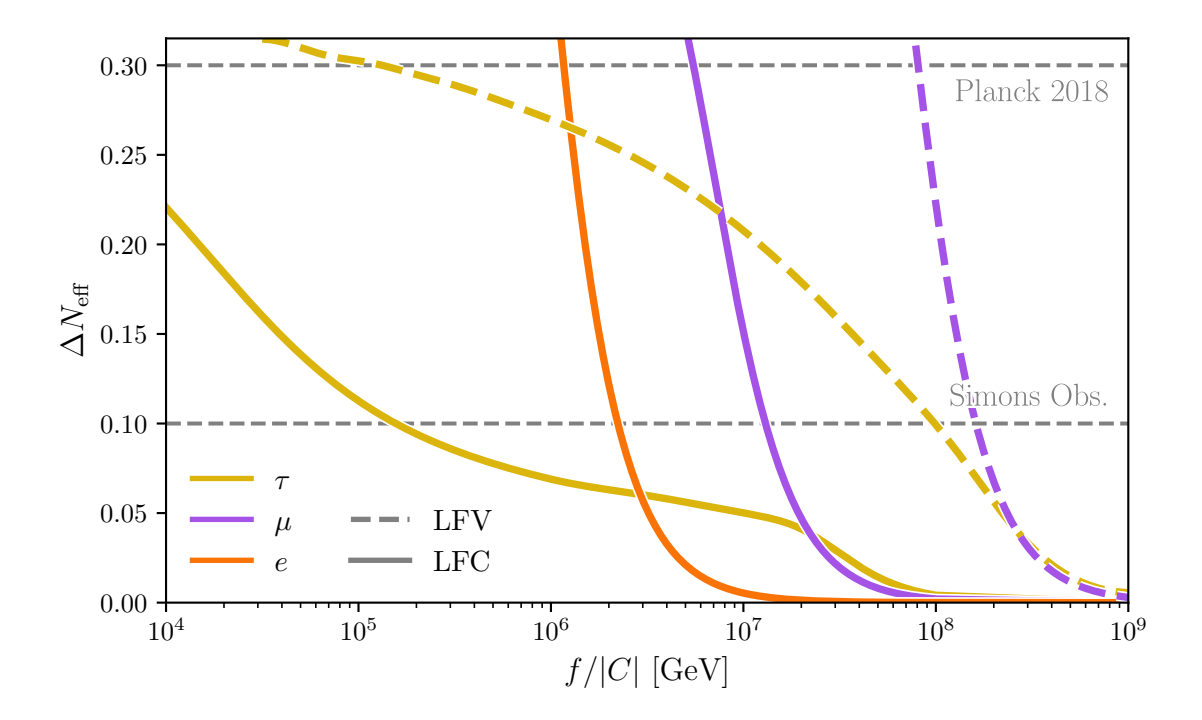


Figure 1: $\Delta N_{\rm eff}$ computed via fBE as a function of f/|C| for all considered lepton channels. Solid curves correspond to lepton-flavor conserving (LFC) processes, while dashed curves correspond to lepton-flavor violating (LFV) processes. The results for electron interactions are plotted with an orange curve (only LFC), muon interactions – with purple curves, and tau interactions – with golden curves. Dashed grey horizontal lines mark the current constraint from Planck and the predicted sensitivity of Simons Observatory. See text for more details.

where ρ_a and ρ_{γ} are the axion energy density and photon energy density, respectively. $\Delta N_{\rm eff}$ effectively parameterizes the impact of additional relativistic species on the sound horizon around recombination, fluctuation amplitude and other cosmological quantities, thus precision CMB measurements and BAO measurements can directly constrain the presence of any excessive radiation density above the SM. For example, the benchmark constraint value established by the Planck analysis is $\Delta N_{\rm eff} \leq 0.3$ at 95% C.L. [33]. In Fig. 1 we show $\Delta N_{\rm eff}$ computed via fBE approach for all axion-lepton couplings that we consider in this work and show the corresponding constraints from Planck and the projected sensitivity of Simons Observatory.

When axion contribution to $\Delta N_{\rm eff}$ is computed it is often assumed that axions were produced in thermal equilibrium and remain ultra-relativistic at the onset of recombination. As demonstrated in Ref. [51] the former assumption (being expressed as the relation between axion number density and energy density) can significantly underestimate the energy density of axions if axion production is rather mild (freeze-in scenario). Furthermore, if axion mass is large enough, the non-relativistic axion species start to dominate the energy density of axions around recombination

$$\rho_a = \frac{g_a T^4}{2\pi^2} \int dq \sqrt{q^2 + \left(\frac{m_a}{T}\right)^2} \cdot q^2 f_a(q)$$
 (2.5)

and $\Delta N_{\rm eff}$ can no longer be used to obtain reliable constraint on the axion decay constant. One can think of a modification to Eq. (2.4) which would take into account only the energy density of relativistic axions at the given temperature. However, the non-relativistic component of the axion gas starts to play its part in the structure formation and leave an imprint on several cosmological observables too. Hence, imposing the constraints on axion models gets more involved than computing just one effective parameter. Still, one may expect that the inclusion of the axion mass makes the constraint stronger than that derived from $\Delta N_{\rm eff}$ for a would-be massless axion, because the axion energy density is enhanced if the axion mass is above the recombination temperature. Indeed, this effect was observed in several detailed analyses of cosmological constraints on QCD axion models, such as KSVZ [47, 48, 54] and DFSZ [54]. Model-independent cosmological constraints including axion mass were also derived on the axion-photon and axion-gluon couplings [55]. However, model-independent cosmological constraints on axion couplings to leptons that take into account the axion mass are missing and our analysis feels this gap.

Moreover, the cosmological effects of the axions also become sensitive to the shape of the momentum distribution $f_a(x,q)$ as it defines the proportions of non-relativistic and relativistic axions. In order to derive cosmological constraints on axion-lepton couplings we do not assume thermal momentum distribution functions, but use those derived from fBE. The cosmological analyses that use non-thermal distributions functions have been performed only for the KSVZ model [47, 48].

3 Cosmological analysis methodology

We consider a cosmological model that extends the standard Λ CDM by incorporating both massive axions and massive neutrinos. The baseline ΛCDM model is typically described by six parameters: the baryon and CDM energy densities, ω_b and $\omega_{\rm cdm}^{-1}$; the scalar amplitude of primordial perturbations A_s ; the scalar spectral index n_s ; the optical depth to reionization τ_{reio} ; and the angular size of the horizon at recombination θ_s . To account for the effects of axions on cosmology we consider two additional parameters: their mass m_a and the inverse strength of their interaction f/|C|, which governs the shape of the axion distribution function $f_a(x,q)$. For neutrinos, we assume three degenerate massive species with a total mass $\sum m_{\nu} \geq 0.06$ eV, consistent with the assumptions made by the Planck Collaboration [33]. Altogether, our extended model $\Lambda \text{CDM} + m_a + f/|C| + \sum m_{\nu}$ includes the six baseline Λ CDM parameters, the sum of neutrino masses (constrained from below as $\sum m_{\nu} \gtrsim 0.06 \,\mathrm{eV}$ [60]), and two axion parameters. This amounts to nine free parameters in total, or eight when the axion mass is fixed. For our numerical analysis we use the Boltzmann-Einstein solver CLASS² [61, 62] to calculate the cosmological observables. To include the non-linear corrections to power spectra we use the halofit routine [63, 64] incorporated into CLASS. We implement the axions originating from lepton processes as an

¹Note that we do not try to explain the observed relic abundance of DM with axions, so $\omega_{\rm cdm}$ denotes a cold DM component of unspecified origin and does not include any contribution from thermally produced axions considered in this paper.

²https://github.com/lesgourg/class_public

Parameter	Prior type	Range
ω_b	flat	[0.005, 0.1]
$\omega_{ m cdm}$	flat	[0, 0.3]
$100 \theta_s$	flat	wide (uninformative)
$\ln(10^{10}A_s)$	flat	wide (uninformative)
n_s	flat	wide (uninformative)
$ au_{ m reio}$	flat	[0.004, 0.8]
$\sum m_{\nu} \text{ [eV]}$	flat	[0.06, 0.3]
Planck nuisance params	Gaussian	official priors

Table 1: Summary of prior ranges adopted in the analysis. Flat priors are assumed unless otherwise specified. The priors on the first six parameters are adopted from the Planck analysis [33]. Planck nuisance parameters are varied with the standard Gaussian priors provided in the official likelihoods. The posteriors of the parameters denoted as "wide (uninformative)" are essentially independent of the priors.

additional non-cold dark matter degree of freedom and modify the code to include axion momentum distribution obtained by solving the fBE [51] (see Appendix A for details). Note that we investigate one axion coupling at a time, setting the others to zero to obtain conservative bounds for each channel.

To constrain the parameter space of our model, we perform Markov Chain Monte Carlo (MCMC) analyses by connecting CLASS to the MontePython sampler³ [65, 66]. We consider two complementary strategies: 1) fixing the axion mass m_a and varying the other parameters (see Section 4); 2) varying all the parameters with m_a having a log-flat prior (see Appendix B). We choose to fix the mass of axions for several reasons: first of all, when the mass is varied across a few orders of magnitude the MCMC scan tends to concentrate in the regions where the likelihood is the highest (below 0.1 eV), which complicates the determination of the f/|C| bound at higher masses. Furthermore, the constraint in this region is already well approximated by the $\Delta N_{\rm eff}$ limit. Fixing the mass allows us to probe the whole mass region more robustly. Second, from the particle physics model-building perspective the axion mass is often a prediction rather than a free parameter (unlike the coupling), hence the first strategy is more aligned with setting cosmological constraints on particular axion models.

We impose priors on all cosmological parameters as summarized in Table 1. The sum of neutrino masses consists of the contributions from three degenerate massive species, each with a mass $m_{\nu} \in [0.02, 0.1]$ eV, such that $\sum m_{\nu} \geq 0.06$ eV. The axion interaction parameter f/|C| is scanned with a log-flat prior, taking $\log_{10}(f/|C|/\text{GeV})$ in the range [4.0, 8.0] for LFC τ couplings, [6.0, 8.0] for LFC e and μ couplings, [7.0, 9.0] for LFV μ couplings, and [4.7, 9.0] for LFV τ couplings. Planck nuisance parameters are varied with the standard Gaussian priors provided in the official likelihoods. For the parameters listed as "wide (uninformative)", we adopt flat priors with ranges chosen sufficiently broad that

³https://github.com/brinckmann/montepython_public

the resulting posteriors are determined entirely by the data.

Our constraints are derived from a combination of CMB and BAO data. For the CMB we use the 2018 Planck likelihoods, including high- ℓ TT, TE, and EE spectra, the low- ℓ temperature and polarization data, as well as the CMB lensing likelihood [56, 57]. For BAO we include the most recent results from the DESI DR2 release [58]. The MCMC chains are obtained via the Metropolis-Hastings algorithm and we consider them to be converged once they reach the Gelman-Rubin convergence criterion R-1 < 0.02. Posterior distributions and confidence intervals are obtained using GetDist⁴ [67].

4 Results

Let us now discuss the results of our cosmological analysis in the form of constraints on axion-lepton couplings for lepton-flavor conserving (LFC) and lepton-flavor violating (LFV) processes separately. In addition, we analyse an approximate bound imposed on massive axions being a form of warm dark matter (wDM) which are relevant for $m_a \gtrsim \mathcal{O}(10)$ eV.

4.1 Lepton-flavor conserving (LFC) interactions

In Figure 2 we present the 95% C.L. limits on $f/|C_i|$ as a function of axion mass for all LFC couplings, shown as colored points connected by solid lines and labeled as CMB+BAO. Each point is the result of a scan with a fixed value of axion mass, from which we obtain the 95% C.L. bound on $f/|C_i|$, and the line simply interpolates between these points. For small axion masses $m_a \lesssim \mathcal{O}(0.1)$ eV axions behave predominantly as dark radiation and are therefore mainly constrained by their contribution to $\Delta N_{\rm eff}$. The cosmological bound increases with the axion mass in all channels up to a few eV. As the mass grows, so does the axion energy density. Thus, to avoid an overproduction of relativistic axions the interaction strength at higher masses must be weaker. In addition, the axion contribution to the late-Universe matter density grows, which implies that a lower density of additional CDM is required to fulfill the observed relic density. As axions with these masses behave as warm DM, they suppress the formation of small-scale structures, which comes in tension with the BAO measurements⁵. Note that in the case of the τ coupling we do not obtain any meaningful 95% C.L. constraints for masses $m_a < 0.12$ eV as the axion abundance in this case is relatively small in comparison to other channels.

As the axion mass grows beyond $\mathcal{O}(10)$ eV, the cosmological constraints begin to weaken. ⁶ In this mass regime, the axions behave predominantly as non-relativistic matter at recombination ($T \approx 0.3$ eV), so their contribution to $\Delta N_{\rm eff}$ is reduced and the bound is relaxed. Consequently, the limits on $f/|C_i|$ become less stringent in this region. In particular this behavior is most pronounced for the τ coupling. This is explained by the

⁴https://github.com/cmbant/getdist

⁵For more information supporting our line of reasoning see Appendix C, in which we show the CMB power spectrum and matter power spectrum predictions for various values of $f/|C_{\tau l}|$ from our scans.

⁶The bounds resulting from our calculations – with and without the halofit procedure for non-linear corrections to power spectra – display a difference of up to a few tens of percent in the considered mass range. Nevertheless, we expect that the actual constraints in this mass range are dominated by the Ly- α forest effects, see Sec. 4.3.

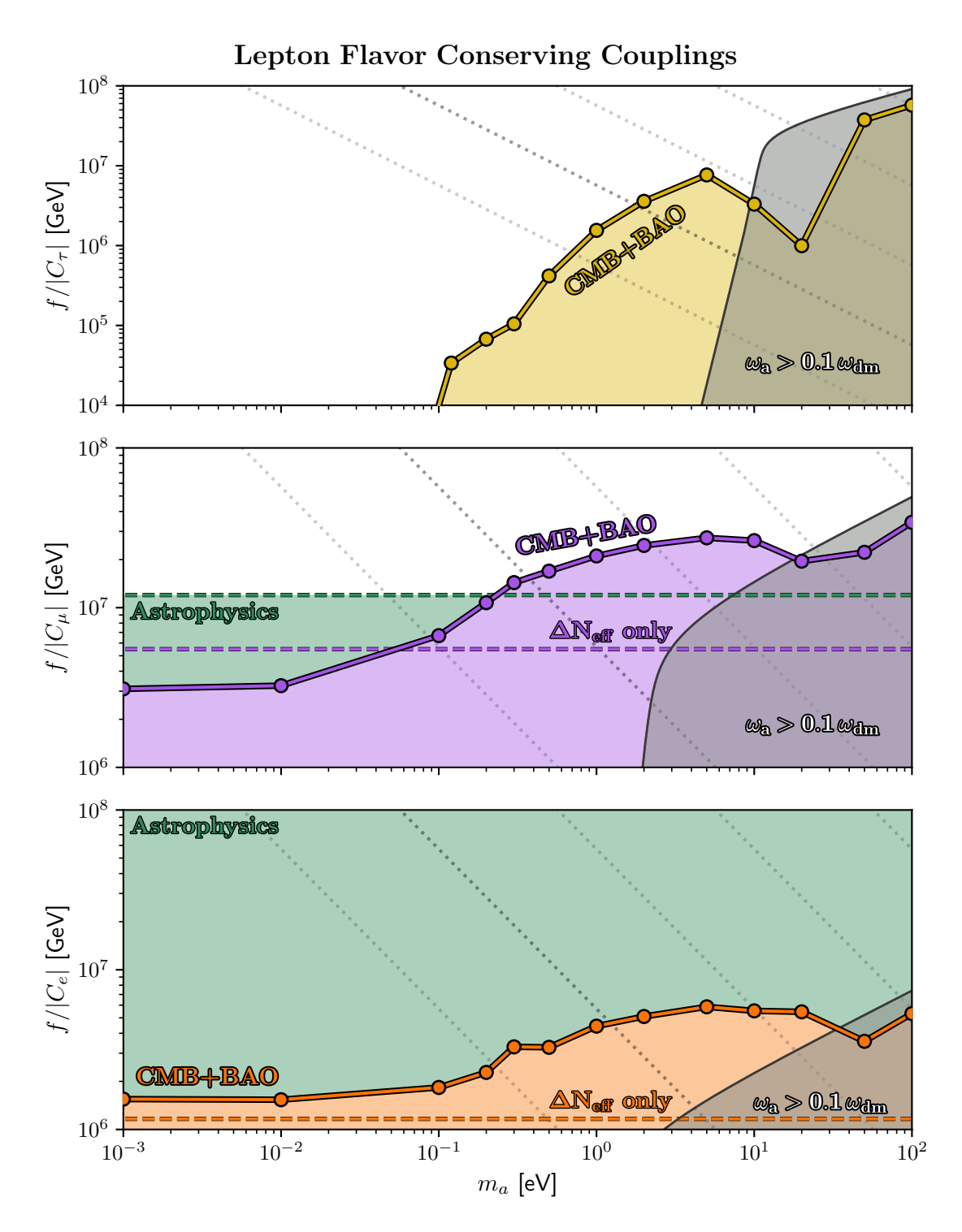


Figure 2: Summary of constraints on LFC axion couplings $f/|C_l|$ as a function of axion mass m_a . The colored points connected with solid lines indicate the 95% C.L lower bounds on the couplings derived from CMB and BAO measurements (Planck 2018 + DESI data). The dashed lines of the same color represent the mass-independent bound on $f/|C_l|$ from the simplified $\Delta N_{\rm eff}$ analysis. The grey region is excluded by the approximate wDM constraint (see Sec. 4.3). Green shading denotes mass-independent astrophysical limits. The dotted lines indicate the cross-sections of the parameter space for the QCD axions with the values of $\log_{10}|C_l|=[-3,-2,-1,0,1]$, from right to left ($|C_l|=1$ is highlighted by a darker color). See the text for more details.

relatively weak dependence of the axion abundance on the value of $f/|C_i|$ for this channel — as can be seen in Fig. 1, even for comparatively large axion masses, there remains a broad range of $f/|C_i|$ values that yield similar cosmological results. Finally, in the limit of large axion mass values $m_a \gtrsim 50$ eV the bound grows stronger again as the abundance of massive axions approaches the observed relic density of CDM or even starts to exceed it.

Around $m_a \sim 10$ eV our constraint becomes comparable to an approximate bound on the allowed fraction of warm DM coming from Ly- α forest observations. Note that we only extrapolate the results of hydrodynamical simulations for particles with $m \sim \mathcal{O}(\text{keV})$, so this bound should be treated simply as an indication that this region is potentially excluded (see Sec. 4.3 for more details).

For the sake of comparison we show the simplified cosmological bounds derived exclusively from the $\Delta N_{\rm eff}$ constraint with the dashed horizontal lines of the same color as the CMB+BAO constraint. These are computed under the assumption that axions remain fully relativistic at recombination and can be compared with the upper limit on $\Delta N_{\rm eff} \leq 0.3$ at 95% C.L. from the Planck analysis (see Sec. 2 and Fig. 1 in particular). Since the axion abundance depends solely on their interaction strength, these bounds are mass independent. The constraint is absent for the τ coupling in the plot as it would fall below the relevant parameter space $f/|C_{\tau}| < 10^4$ GeV. While the limits obtained with each approach are very similar for small axion masses⁷, at higher masses our full analysis predictably provides stronger constraints than the simplified approach. This highlights the importance of properly accounting for the axion mass and for the transition from the relativistic to the non-relativistic regime.

In addition we show the complementary astrophysical constraints on the interaction strength as green dash-dotted lines and the shaded region of the corresponding color to highlight the excluded parameter space. The electron and muon couplings are constrained by the distinct astrophysical observations: the observed shape of the white dwarf luminosity function [69] and the energy-loss argument for SN1987A [70], respectively. These yield the following 95% C.L. limits:

$$\frac{f}{|C_e|} \gtrsim 2 \times 10^9 \text{ GeV},$$
 $\frac{f}{|C_\mu|} \gtrsim 1.2 \times 10^7 \text{ GeV}.$ (4.1)

In contrast, there is no strong astrophysical bound for τ coupling as this type of leptons typically plays a very small role in astrophysical processes. The axion- τ coupling can be constrained indirectly by the astrophysical bound on axion-electron coupling since the latter is generated by the τ coupling at one-loop level. This results in a lower bound on $f/|C_{\tau}|$ at the level of a few times 10^4 GeV [38]. We do not show this bound in Figure 2 since its exact value depends on the UV cut-off of low-energy theory, so it is model-dependent.

Our cosmological analysis provides the most stringent limit to date on the τ coupling for axion masses above $\mathcal{O}(0.1)$ eV and the values of $f/|C_{\tau}|$ of up to $\mathcal{O}(10^7)$ GeV are excluded for

⁷The constraints on axion couplings stemming from $\Delta N_{\rm eff} \leq 0.3$ are typically stronger than those derived by us from Planck and DESI data for $m_a \ll 0.1$ eV (the only exception being the constraints on $f/|C_e|$ which is an artifact resulting from our choice of the prior and a very steep dependence of $\Delta N_{\rm eff}$ on $f/|C_e|$). This is because the inclusion of DESI results relaxes the upper bound on $\Delta N_{\rm eff}$, as was already observed e.g. in Ref. [68].

 m_a in the eV range. For the μ coupling our results are competitive with the astrophysical constraint and for axion masses above 0.2 eV our bound can even surpass it, excluding $f/|C_{\mu}|$ below a few times 10⁷ GeV. On the other hand, the astrophysical bound for the electron coupling is much stronger than that from cosmology.

Our results have also implications for the QCD axion. The dotted grey lines in Fig. 2 show the cross sections of the parameter space that correspond to the QCD axions for which the relation in Eq. (1.1) holds for various values of C_l . Thus, for QCD axions with $|C_l| \leq 1$ our results provide stronger constraints on f compared to the mass-independent $\Delta N_{\rm eff}$ limits for all channels and the strongest constraints in general for axion couplings to muons and tau leptons. In particular, for $C_{\tau}=1$ cosmology excludes the values of $m_a \gtrsim 2$ eV, or equivalently, $f \lesssim 3 \times 10^6$ GeV, which would otherwise be unconstrained if naive $\Delta N_{\rm eff}$ constraint was applied. For $C_{\mu}=1$, $m_a \gtrsim 0.4$ eV and $f \lesssim 1.5 \times 10^7$ GeV are excluded, which is an improvement of about a factor of three with respect to the constraint from $\Delta N_{\rm eff}$ that neglects the mass of the axion. For $C_e=1$, the lower bound on f is improved to about 5×10^6 GeV, but it is still weaker than the astrophysical bound by almost three orders of magnitude.

4.2 Lepton-flavor violating (LFV) interactions

In Figure 3 we present the 95% C.L. limits for the LFV couplings. As the axion distribution functions for τ decays into electrons and muons are virtually indistinguishable we display only one plot with the constraints on $f/|C_{\tau l}|$, where l is μ or e. Our limits demonstrate qualitatively similar behaviour to the ones obtained for LFC couplings and can be explained via the same physical reasoning. We also show the $\Delta N_{\rm eff}$ limits, and the comparison between these simplified constraints and our full cosmological constraints reaches the same conclusion as for the LFC case: the limits at low masses are comparable, while at higher masses the simplified limits are much weaker. Instead of the astrophysical bounds as in the LFC case, the LFV couplings are constrained by the collider measurements and the respective limits are shown as red dash-dotted lines. For the tau couplings, the limits are set by Belle-II [71]; for the muon couplings, they are derived from the TRIUMF and TWIST experiments [72, 73]. The corresponding current bounds at 95% C.L. are:

$$\frac{f}{|C_{\tau e}|} \gtrsim 4.6 \times 10^6 \,\text{GeV}, \qquad \frac{f}{|C_{\tau \mu}|} \gtrsim 3.6 \times 10^6 \,\text{GeV}, \qquad \frac{f}{|C_{\mu e}|} \gtrsim 5 \times 10^8 \,\text{GeV}.$$
 (4.2)

The collider bound on $C_{\mu e}$ depends on the chirality structure. The bound quoted above assumes purely left-handed coupling, corresponding to $C_{\mu e}^{V} = -C_{\mu e}^{A}$, which is weaker than that for purely right-handed coupling by a factor of about 2.5 [74].

The most significant impact of the axion mass on the cosmological bound can be seen for the LFV axion couplings involving τ lepton. Our cosmological bounds for τ couplings are competitive with the collider limits and even supersede them for axion masses above 0.3 eV. For masses above about 1 eV the lower bound on $f/|C_{\tau l}|$ exceeds 10^8 GeV, which is an order of magnitude stronger than a projected future bound from Belle-II with 50ab^{-1} of data estimated to be $f/|C_{\tau l}| \gtrsim 2 \times 10^7$ GeV [19]. The cosmological bound on the QCD axions with $|C| \leq 1$ is the strongest of all for τ couplings, which for $C_{\tau l} = 1$ corresponds

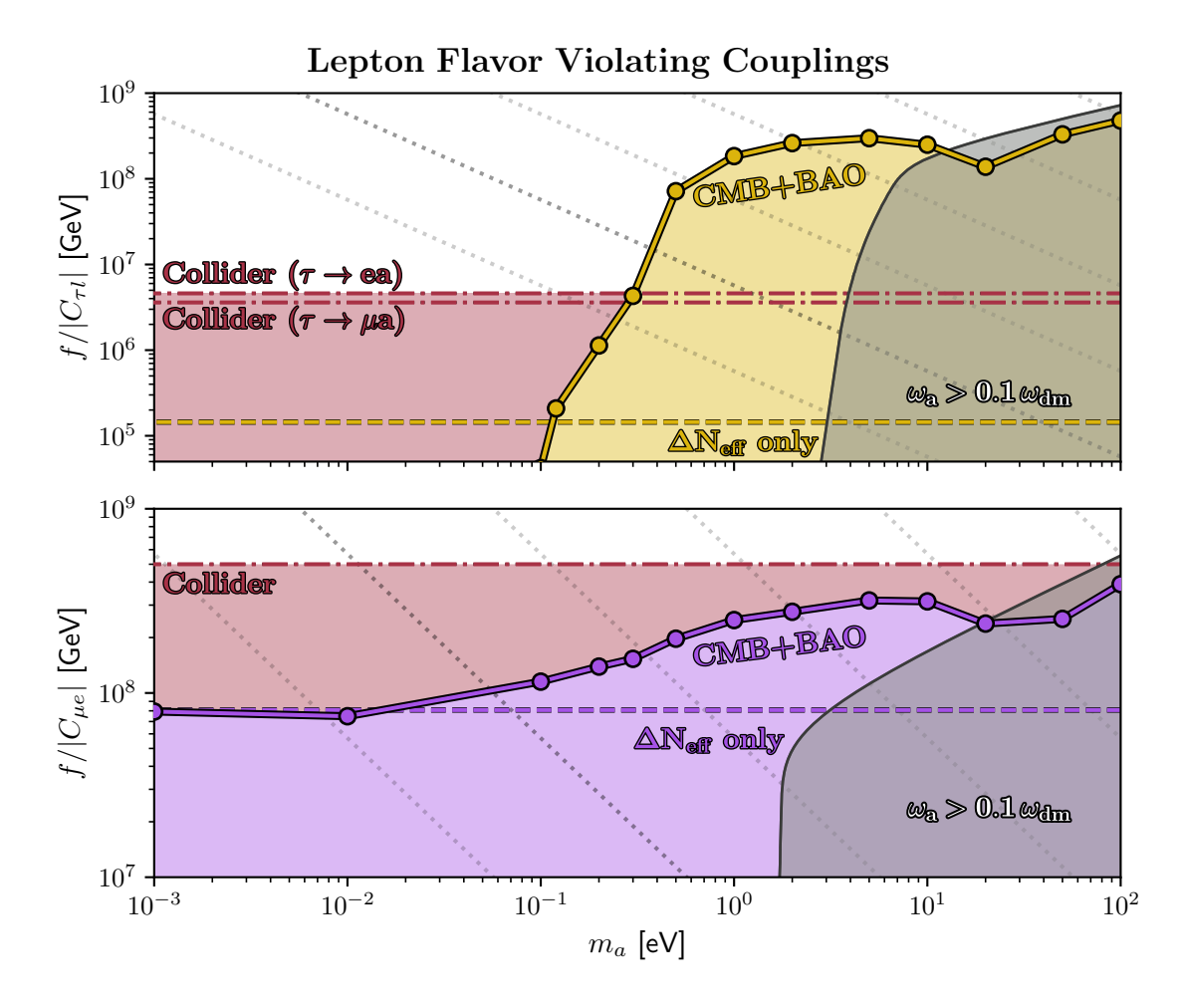


Figure 3: Same as Fig. 2, but for LFV axion couplings.

to $m_a \lesssim 0.4$ eV, or equivalently, $f \gtrsim 2 \times 10^7$ GeV. On the other hand, for LFV axion- μ -e coupling the collider bounds remain stronger than cosmological constraints over the entire mass range considered in our analysis with CLASS. Nevertheless, for $m_a \gtrsim 100$ eV we expect that the constraints on axions from Ly- α forest may become stronger than the collider ones.

Let us also compare our results with those of Ref. [75], which investigated cosmological constraints on light, but massive thermal relics that decoupled from the SM plasma before the EW phase transition. Even though Ref. [75] adopted instantaneous decoupling approximation it is still possible to approximately translate their upper bounds on the temperature of light relics into bounds on axion couplings. We find a good agreement for axion masses up to 1 eV. For larger axion masses, up to 10 eV, our bounds are somewhat weaker than those inferred from the results of Ref. [75]. While a strict comparison of the results is not possible, as we used the latest DESI data instead of the BOSS data employed in Ref. [75], they argue that the inclusion of additional weak-lensing data [76] and, to a lesser extent, of the full-shape galaxy data improves the upper bounds on the energy density of light relics by a factor of a few. Thus, our bounds for axion masses above 1 eV should be regarded as conservative. We expect that incorporating the weak-lensing data may improve bounds on

some axion couplings by up to a factor of a few in this mass range. We leave a detailed investigation of this effect for future work.

4.3 Warm DM constraint

In addition to the impact on the early structure formation, that can be probed by CMB and BAO measurements, axions with masses $m_a \lesssim \mathcal{O}(10)$ keV are also expected to have an effect on the late-time structure formation probed by Ly- α forest observations. In other words, it means that these axions behave as warm dark matter. While the former effects on the cosmological observables can be reliably computed in the linear regime using CLASS, the latter effects require hydrodynamical simulations. We use the results of these simulations from the literature in order to estimate the wDM constraints on the axion abundance. These constraints can be conveniently expressed in terms of the fraction of warm axion contribution to the total dark matter energy density $f_{\text{wdm}} \equiv \omega_a/\omega_{\text{dm}}$, where $\omega_a \equiv \Omega_a h^2$ is the axion contribution to the energy density of the Universe.

The results of Ref. [77] suggest that below $m_a \sim 5$ keV the upper limit on $f_{\rm wdm}$ decreases and reaches $f_{\rm wdm} = 16\%$ at 1 keV, which is the minimum of the mass range in that analysis. The authors state that the upper limit should keep decreasing towards smaller masses, however it is expected to ultimately reach a plateau due to the fact that the Ly- α data becomes insenstive to wDM effects. Ref. [78] reaches a qualitatively similar conclusion and states that any mass of a new particle is allowed by the Ly- α data as long as it constitutes less than 10% of the total DM density. Thus, we conservatively estimate the wDM constraint on the axions with the masses $m_a < 1$ keV as $f_{\rm wdm} \le 0.1$.

For the range of axion masses in our analysis one can confidently use the non-relativistic approximation for the present-day axion energy density

$$\rho_a(T_0) \simeq m_a \cdot n_a(T_0) \,, \tag{4.3}$$

where n_a is the axion number density and T_0 is the present temperature of the Universe (CMB). In the fBE approach that we concentrate on in this paper the present-day axion number density can be calculated from the axion distribution function f_a as follows

$$n_a(T_0) = \frac{g_a}{2\pi^2} T_0^3 \left(\frac{h_s(T_d)}{h_s(T_0)}\right)^{-1} \int_0^\infty \tilde{q}^2 f_a(\tilde{q}) d\tilde{q}, \tag{4.4}$$

where $\tilde{q} \equiv q \cdot (h_s(T_0)/h_s(T_d))^{-1/3}$ is the reduced momentum coordinate which preserves the same shape of the axion distribution function across the entropy density evolution in the expanding Universe in the absence of axion interactions [51] and T_d is the temperature at which $f_a(q)$ is obtained⁸. In the nBE approach the present-day axion density is obtained straightforwardly from the solution of the Boltzmann equation for the comoving abundance of axions Y_a as

$$n_a(T_0) = Y_a \cdot s_0 \,, \tag{4.5}$$

where s_0 is the present-day CMB entropy density.

⁸In our analysis we trace the evolution of $f_a(x,q)$ until x=20, at which the axion comoving abundance is firmly established.

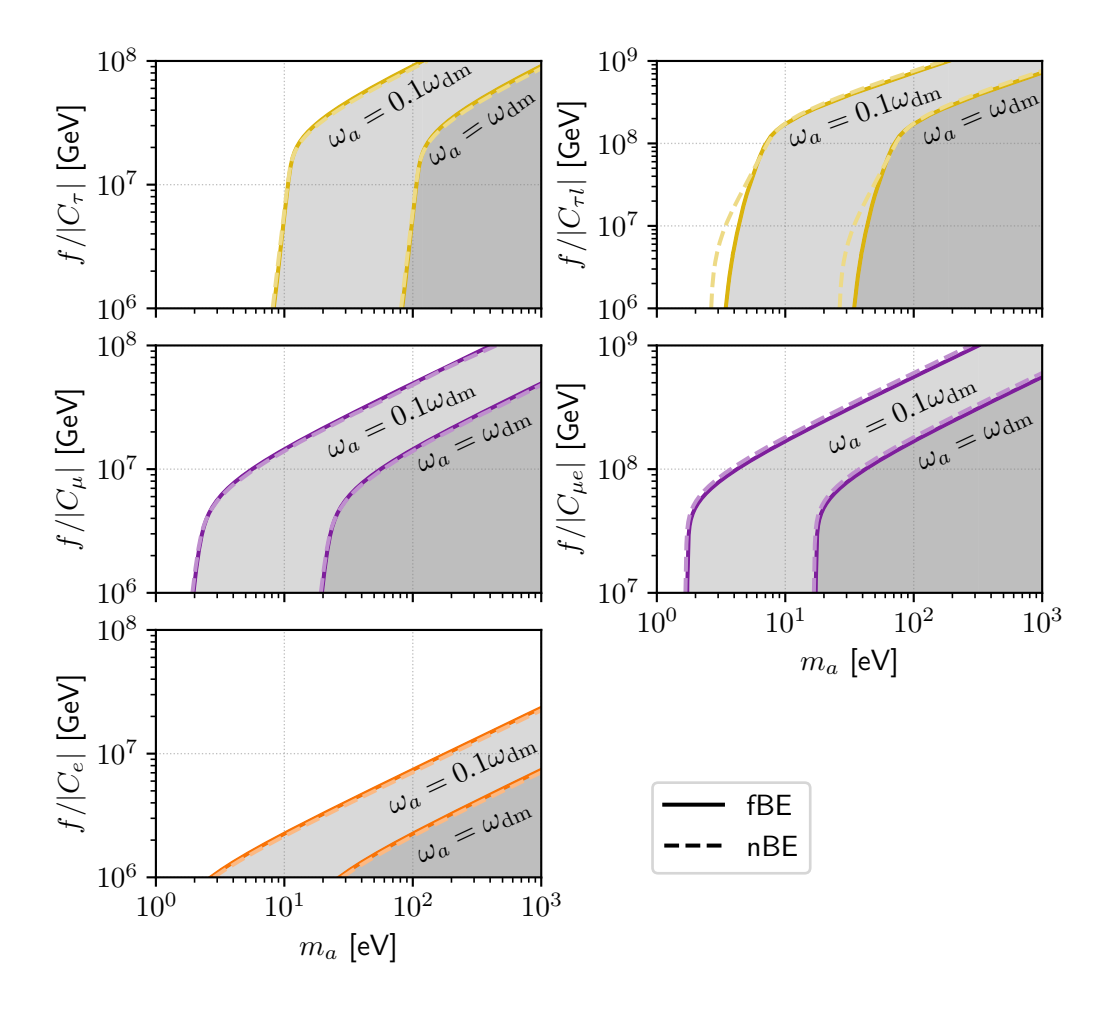


Figure 4: Constraints on the axion decay constant f/|C| as a function of the axion mass m_a from the axion contribution to the present-day DM abundance, $\omega_{\rm dm}=0.12$. Each panel corresponds to a distinct axion-lepton interaction with LFC (LFV) interactions shown on the left (right) panels. Solid lines correspond to the calculation of the axion abundance via fBE approach, while the dashed lines correspond to the nBE approach. We show two contours of the present-day axion energy density: $\omega_a = \omega_{\rm dm}$ (CDM bound) and $\omega_a = 0.1\omega_{\rm dm}$ (wDM bound). The shaded region below the $\omega_a = 0.1\omega_{\rm dm}$ indicates the parameter space that we estimate to be excluded due to overproduction.

With these expressions we trace which combinations of m_a and f/|C| (that solely determines the axion abundance in the thermal scenario) result in $\omega_a = 0.12$ and $\omega_a = 0.012$. The first value corresponds to the whole observed DM abundance, while the second value corresponds to 10% of the observed DM abundance, thus comprising the strong bound on the axion abundance from overclosing the Universe and a conservative estimate of the bound from Ly-alpha constraints. These bounds are presented in Fig. 4 for different axion-lepton production channels. Each bound is computed for both fBE and nBE approaches. The bounds in the plots constrain the regions of the axion parameter space located below the contours. The lower is m_a the higher is the allowed comoving density of axions (see Eq. (4.3)). Consequently, the corresponding value of f/|C| required to reproduce this

density is reduced, which explains the downward trend of the constraint curves shown in the plots. The knees of the curves indicate the transition from freeze-in regime at large f/|C| to freeze-out regime at small f/|C|. The only substantial difference between the nBE and fBE constraints is observed for τ decays, which is due to a smaller axion number density found with the fBE approach. This is basically the consequence of the decay kinematics (large non-thermal corrections due to the mass difference) and the rapid change of entropy degrees of freedom around the freeze-out⁹.

A recent work [27] investigated in detail the constraints on the mass of axions playing the role of warm DM, while taking into account the phase-space distributions of axions produced in leptonic channels via freeze-in. The lower bound on the axion mass was found to be between 20 and 40 keV with the exact value dependent on the axion production channel. Ref. [27] also concluded that axions produced thermally in leptonic channels can play the role of DM¹⁰ except for the case when axion couples to electrons, in which axion DM is excluded by X-ray constraints because of too large an axion-photon coupling induced at one loop by the axion-electron coupling. Figure 4 shows complementary results for $m_a < 1$ keV for which thermally produced axions cannot explain all the observed dark matter, but are stable enough to avoid X-ray constraints and the strongest bounds are those from Ly- α forest constraints, which we approximate in this mass region demanding $\omega_a < 0.1 \omega_{\rm dm}$. We see that the lower bounds on f/|C| for LFC axion couplings to muons and taus exceed 10⁸ GeV, while those for LFV axion couplings exceed 10⁹ GeV for axion masses approaching 1 keV and are stronger than astrophysical and collider constraints. The lower bound on $f/|C_e|$ for $m_a \approx 1$ keV exceeds 10^7 GeV, but it is still much weaker than the astrophysical bound.

5 Conclusions

We have investigated cosmological constraints on axion-lepton interactions using state-ofthe-art computations of axion momentum-distribution functions arising from axions thermally produced in the SM bath. We used the CMB measurements from Planck together with the BAO results from DESI DR2 to constrain both LFC and LFV axion couplings. Our results strengthen the existing cosmological bounds, that have been derived using upper bounds on $\Delta N_{\rm eff}$, in the range of axion masses between about 0.1 eV and 1 keV.

Figure 5 exemplifies the impact of non-vanishing axion mass on the constraints on axion-lepton couplings. We compare the constraints derived from the Planck upper bound on $\Delta N_{\rm eff} < 0.3$, which is valid under the assumption of negligible axion mass, with the constraints for $m_a = 0.3$ eV and $m_a = 10$ eV. We see that already for $m_a = 0.3$ eV, when the axion mass is close to the recombination temperature, our constraints on axion-lepton couplings are significantly stronger than those derived from the upper bound on $\Delta N_{\rm eff}$. For $m_a = 10$ eV, which is in the ballpark of axion masses maximizing the constraints, the bounds are improved by a factor of about 5 for LFC axion couplings to electrons and muons

⁹For more details see Ref. [51], especially Fig. 2 and the text around it.

 $^{^{10}}$ In an earlier work [25], a detailed phenomenological analysis of thermally produced axion DM via the decay $\mu \to ea$ was carried out.

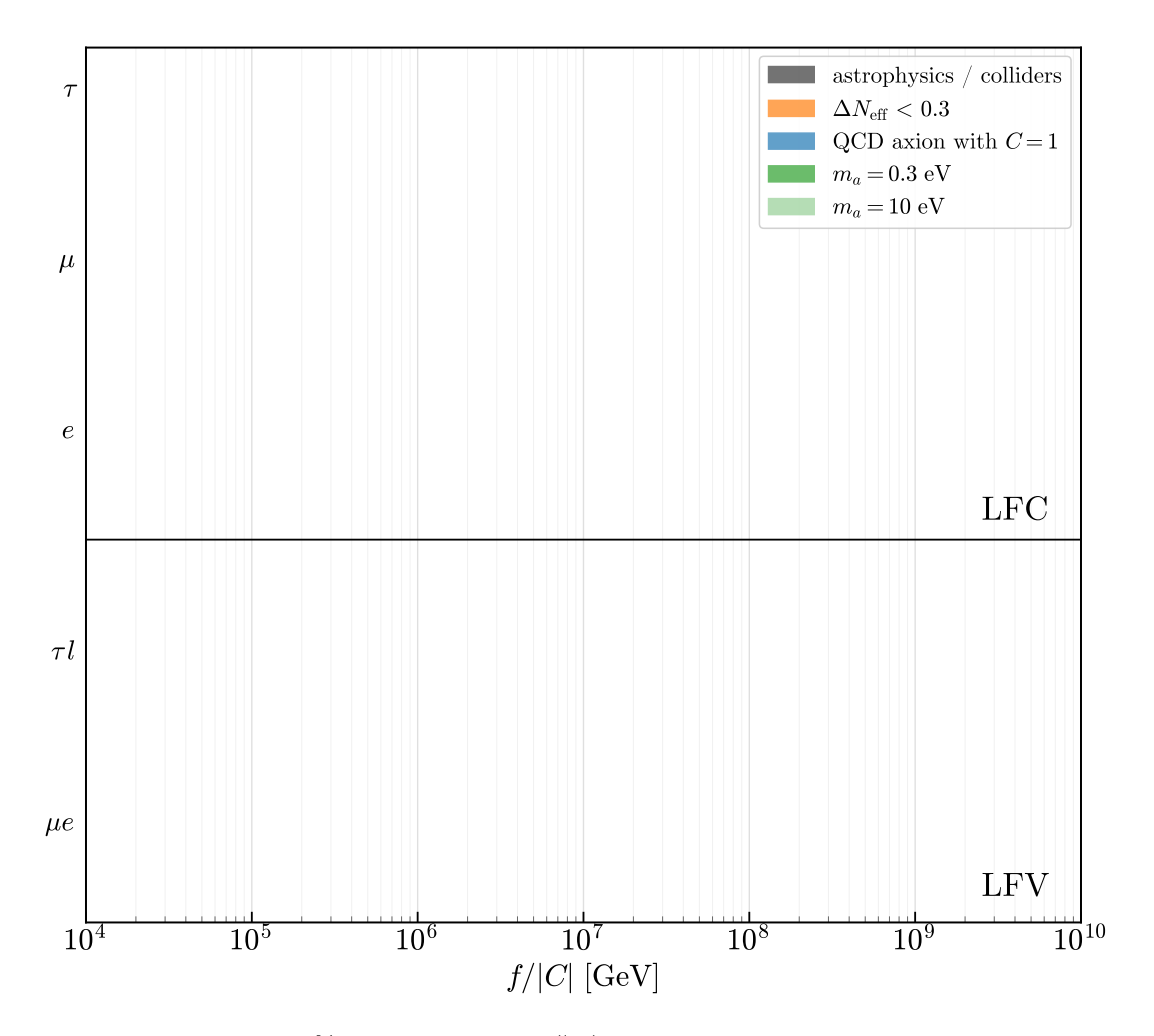


Figure 5: Summary of 95% C.L. bounds on f/|C| for LFC and LFV axion-lepton couplings. The orange bars represent the weakest cosmological limits based on the upper bound on $\Delta N_{\rm eff} < 0.3$ from Planck. Blue bars show the bounds for the axion decay constant for a QCD axion with C=1, while green bars illustrate two representative scenarios with non-vanishing axion mass, $m_a=10~{\rm eV}$ and $m_a=0.3~{\rm eV}$. The strongest non-cosmological constraints are represented by the dark–grey bars and correspond to astrophysical (collider) bounds for LFC (LFV) couplings.

and LFV ones to muon and electron, while the bound on LFC and LFV axion couplings involving tau leptons are improved by many orders of magnitude. For axion masses above about 10 eV we expect that the strongest cosmological constraints are those from Ly- α forest, since axion in this mass range behaves like warm DM. The derivation of precise constraints from it is beyond the scope of this paper, but we derive approximate constraints relying on the computation of axion abundance. These constraints become stronger with increasing m_a and become the strongest for $m_a \sim \mathcal{O}(1)$ keV.

For large enough masses, the cosmological constraints are also typically stronger than those from colliders and astrophysics. Cosmology provides the most stringent constraints on LFC axion couplings to taus and muons for axion masses above about 0.1 and 0.3 eV, respectively. The lower bounds on $f/|C_{\tau}|$ and $f/|C_{\mu}|$ range from about 10^4 and 10^7 GeV,

respectively, for $m_a \sim \mathcal{O}(0.1)$ eV up to about 10^8 GeV for $m_a \sim \mathcal{O}(1)$ keV, where the axion contribution to warm DM is strongly constrained by Ly- α forest. The constraints on axion-electron couplings are not competitive with astrophysical constraints and the lower bound from cosmology on $f/|C_e|$ varies from about 10^6 GeV for very light axions up to about 10^7 GeV for $m_a \sim \mathcal{O}(1)$ keV.

For LFV axion couplings we found the lower cosmological bound on $f/|C_{\tau e}|$ and $f/|C_{\tau \mu}|$ to be stronger than the collider limits from Belle-II for axion masses above about 0.3 eV and this bound exceeds 10^9 GeV for $m_a \sim \mathcal{O}(1)$ keV. Since the collider bounds on LFV axion couplings to muon and electron are very strong, cosmology cannot compete with them for light axions, but for axion masses above about 100 eV cosmological constraints become stronger and the lower bound on $f/|C_{\mu e}|$ exceeds 10^9 GeV for $m_a \sim \mathcal{O}(1)$ keV.

Our results can be also applied to the QCD axion. We see in Figure 5 that for axion-lepton couplings with $C \sim \mathcal{O}(1)$ the bounds on the axion decay constant are stronger than the simplified ones derived from the upper bound on $\Delta N_{\rm eff}$. The strongest cosmological constraints are for the QCD axions with sizable LFC couplings to muons or LFV couplings involving tau, for which the values of the axion decay constant above 10^7 GeV are excluded. Although astrophysical constraints on the QCD axion couplings to nucleons often lead to stronger bounds on f, in some astrophobic QCD axion models [13, 19] our cosmological constraints provide the strongest lower bound on the axion decay constant.

Acknowledgments

The authors would like to thank Daniele Perri and Olga Garcia-Gallego for useful discussions. This work was partially supported by the National Science Centre, Poland, under research grant no. 2020/38/E/ST2/00243.

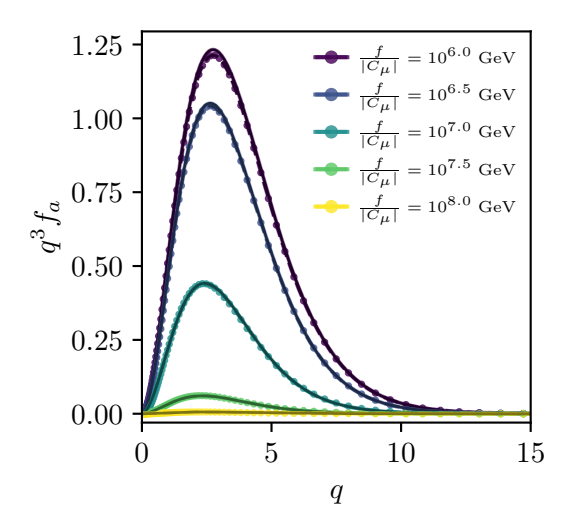
A Implementation of axion distribution functions in CLASS

In this Appendix we describe in detail how we implement axion distribution functions in CLASS. The fBE for the axion energy distributions $f_a(q)$ is solved numerically for a range of discrete values of axion interaction strength f/|C| as in Ref. [51], thus we obtain a set of tabulated distributions for each value considered. While CLASS can in principle process such tabulated results for fixed values of f/|C|, this is insufficient for our purposes: to constrain the axion coupling with cosmological data we need to explore arbitrary values of f/|C| in our MCMC analyses. To achieve this we perform analytical fits to the numerically obtained distributions. We find that they are well approximated by the following functional form

$$q^2 f_a(q) = \sqrt{1+q^2} \ q^d \left(\exp\left(A\sqrt{1+q^2}-M\right) + k\right)^{-1},$$
 (A.1)

where $q \equiv E_a/T$ and the parameters $\alpha \equiv \{A, M, k, d\}$ are smooth functions of the interaction strength. In particular, they can be expressed as polynomials in $\log f/|C|$:

$$\alpha_i(f/|C|) = b_0 + b_1 \log f/|C| + b_2(\log f/|C|)^2 + \dots$$
 (A.2)



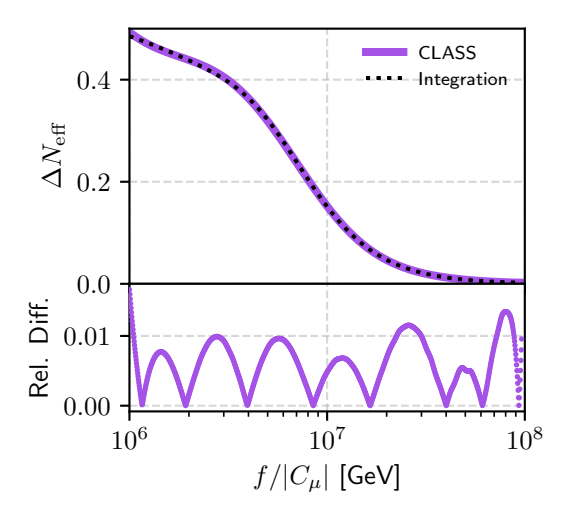


Figure 6: Left: Comparison of the axion momentum distributions resulting from LFC μ interactions for different values of $f/|C_{\mu}|$ and their fitting functions. The points correspond to the distributions obtained numerically, the dashed lines to the initial fits to these distributions and the solid lines to the final fit, as explained in the text. Right: $\Delta N_{\rm eff}$ calculated by integrating the numerical distributions (black dashed line) and obtained from CLASS with the procedure explained in this appendix (purple line). The lower panel shows the relative differences between these two approaches.

with b_i being some coefficients obtained via fitting. Therefore, our procedure consists of two steps:

- 1. For each value of f/|C|, we fit the function (A.1) to the numerical distribution, obtaining a set of parameters $\{A, M, k, d\}$.
- 2. The resulting parameters are then fitted using (A.2), providing a continuous mapping between f/|C| and the distribution function.

As an illustration, in the left panel of Fig. 6 we present the results for the LFC axion-muon coupling. The points correspond to a numerical solution of the fBE, the dashed lines to the initial fits from the first step, and the solid lines to the final distributions obtained after implementing the parameter fits. We see that the fitted functions agree very well with the numerical results. As a cross-check, the right panel shows the resulting values of $\Delta N_{\rm eff}$: the dotted black line corresponds to the values obtained by integrating the numerical distributions directly, while the solid light purple line shows the results from CLASS obtained with our fitted functions. The lower panel shows the relative difference between the two approaches. Once again, we observe a good consistency between the results of using actual distributions and the results of using fitting functions, confirming that our implementation is suitable for MCMC scans.

Parameter	au LFV	μ LFV	au LFC	μ LFC	e LFC
$10^2 \omega_{ m b}$	$2.264^{+0.028}_{-0.028}$	$2.259^{+0.027}_{-0.026}$	$2.260^{+0.027}_{-0.026}$	$2.258^{+0.030}_{-0.027}$	$2.256^{+0.027}_{-0.025}$
$\omega_{ m cdm}$	$0.1198^{+0.0032}_{-0.0032}$	$0.1184^{+0.0038}_{-0.0025}$	$0.1188^{+0.0028}_{-0.0022}$	$0.1188^{+0.0058}_{-0.0028}$	$0.1179^{+0.0026}_{-0.0021}$
$ heta_{s,100}$	$1.04176^{+0.00070}_{-0.00069}$	$1.04196^{+0.00065}_{-0.00068}$	$1.04191^{+0.00058}_{-0.00062}$	$1.04191^{+0.00071}_{-0.00082}$	$1.04203^{+0.00057}_{-0.00065}$
$\ln 10^{10} A_s$	$3.060^{+0.032}_{-0.030}$	$3.056^{+0.031}_{-0.028}$	$3.057^{+0.031}_{-0.028}$	$3.059^{+0.033}_{-0.030}$	$3.055^{+0.031}_{-0.029}$
n_s	$0.9750^{+0.0089}_{-0.0090}$	$0.9723^{+0.0084}_{-0.0081}$	$0.9731^{+0.0078}_{-0.0074}$	$0.972^{+0.011}_{-0.0090}$	$0.9713^{+0.0074}_{-0.0075}$
$ au_{ m reio}$	$0.061^{+0.016}_{-0.014}$	$0.061^{+0.016}_{-0.014}$	$0.061^{+0.015}_{-0.014}$	$0.062^{+0.016}_{-0.014}$	$0.062^{+0.016}_{-0.014}$
$\log_{10}\left(m_a/\mathrm{eV} ight)$	< -0.263	_	< -0.225	_	—
$\log_{10}\left(f/ C /\mathrm{GeV} ight)$	_	> 7.98	_	> 6.58	> 6.25
$\Sigma m_ u [{ m eV}]$	< 0.119	< 0.114	< 0.115	< 0.111	< 0.115

Table 2: Best fit values and 95% Confidence Limits for the scanned cosmological parameters.

B Results of full scans with varying axion mass

In this Appendix we present the results of the full cosmological scans in which we treat m_a as a free parameter and scan over it in the range $[10^{-3}, 10]$ eV. Our upper bound on the axion mass prior is only 10 eV, because for larger masses the constraints from Ly- α forest are expected to be stronger than those from CMB and BAO. Similarly to the analysis described in the main text, we consider our scans converged once they reach the Gelman-Rubin factor R-1<0.02. In Fig. 7 we show the preferred regions in the f/|C|- m_a plane for LFC and LFV couplings obtained after marginalizing over all other cosmological and nuisance parameters. In Table 2 we list the best-fit values and 95% limits for the scanned cosmological parameters.

In Fig. 8 we show 1D and 2D posterior distributions (triangle plots) for all the cosmological parameters and axion parameters resulting from our full scans with varying axion mass. The lower left triangle corresponds to LFC couplings, while the upper right triangle corresponds to LFV couplings, and different colors denote different lepton modes. Darker and lighter shadings in 2D plots correspond to 1σ and 2σ regions respectively. In 1D plots the likelihoods for LFC couplings are plotted with solid lines and with dashed lines for LFV couplings. The dashed lines in 1D and 2D plots for f/|C| parameter indicate the boundaries on the priors for different lepton channels. Note that f/|C| vs. m_a plots in this section should not be compared with our constraints described in the main text (e.g. Fig. 2), as those results correspond to a different type of scans with fixed axion masses.

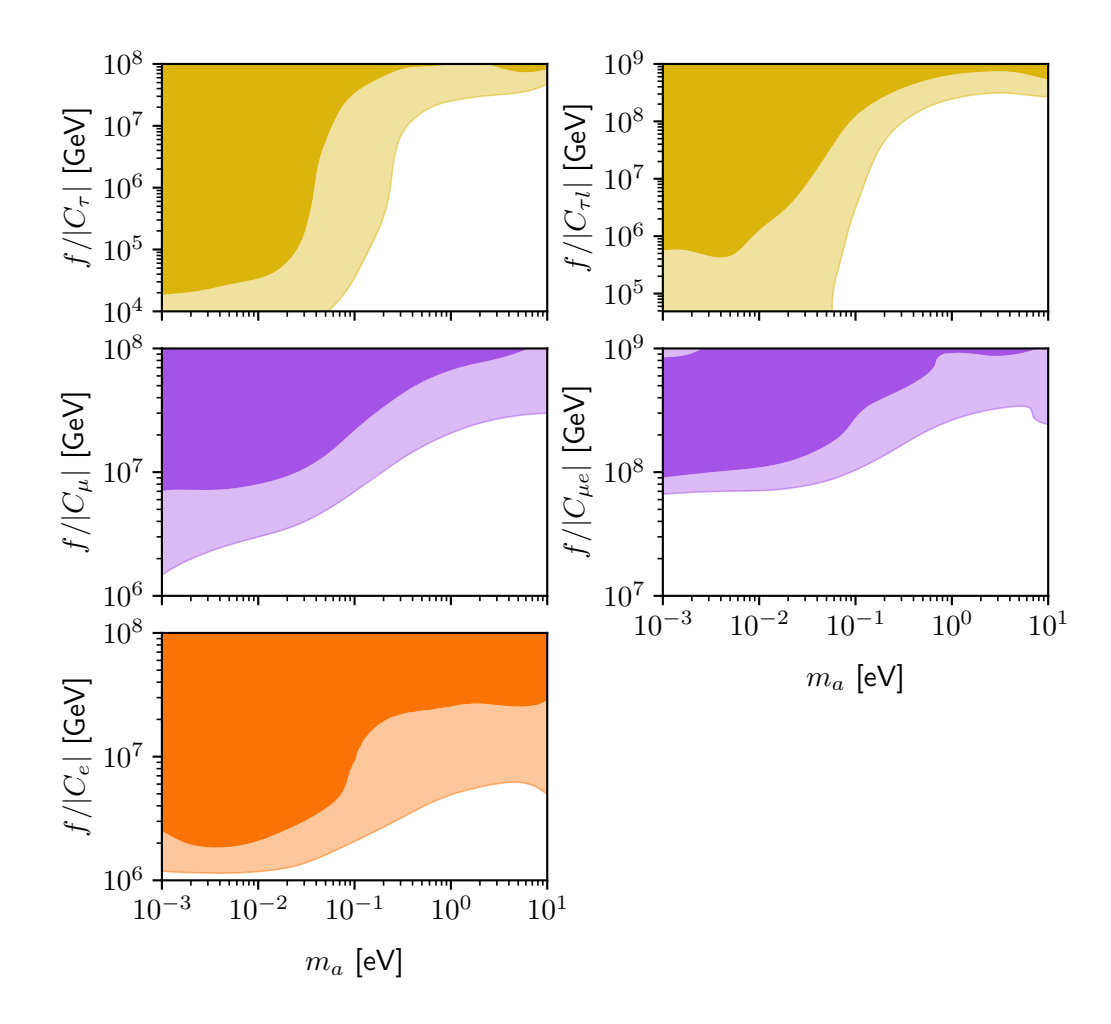


Figure 7: Posteriors of the full cosmological scans in the plane f/|C|- m_a with varying axion mass m_a for all considered channels of axion production. Darker and lighter color shadings indicate 1σ and 2σ regions respectively.

C CMB power spectrum and matter power spectrum for τ decays

In this Appendix we show the predictions from various axion models that we include in our MCMC scans on the example of axion-tau LFV processes. We choose this particular channel for the purpose of demonstration as it usually yields the most pronounced effects comparing to other axion-lepton channels.

We consider three observable quantities: temperature power spectrum C_ℓ^{TT} , lensing power spectrum $C_\ell^{\phi\phi}$ and matter power spectrum P(k). As the main motivation of our analysis is to set constraints on axion models, it is more convenient to show the *deviations* of these quantities from the Λ CDM predictions, e.g. $\Delta D_\ell^{ii} \equiv D_\ell^{ii}(f/|C_{\tau\ell}|) - D_{\ell,\Lambda\text{CDM}}^{ii}$, where we defined

$$D_{\ell}^{TT} = \frac{\ell(\ell+1)C_{\ell}^{TT}}{2\pi}T_0^2, \qquad D_{\ell}^{\phi\phi} = 10^7 \frac{\ell^2(\ell+1)^2}{2\pi}C_{\ell}^{\phi\phi}, \qquad (C.1)$$

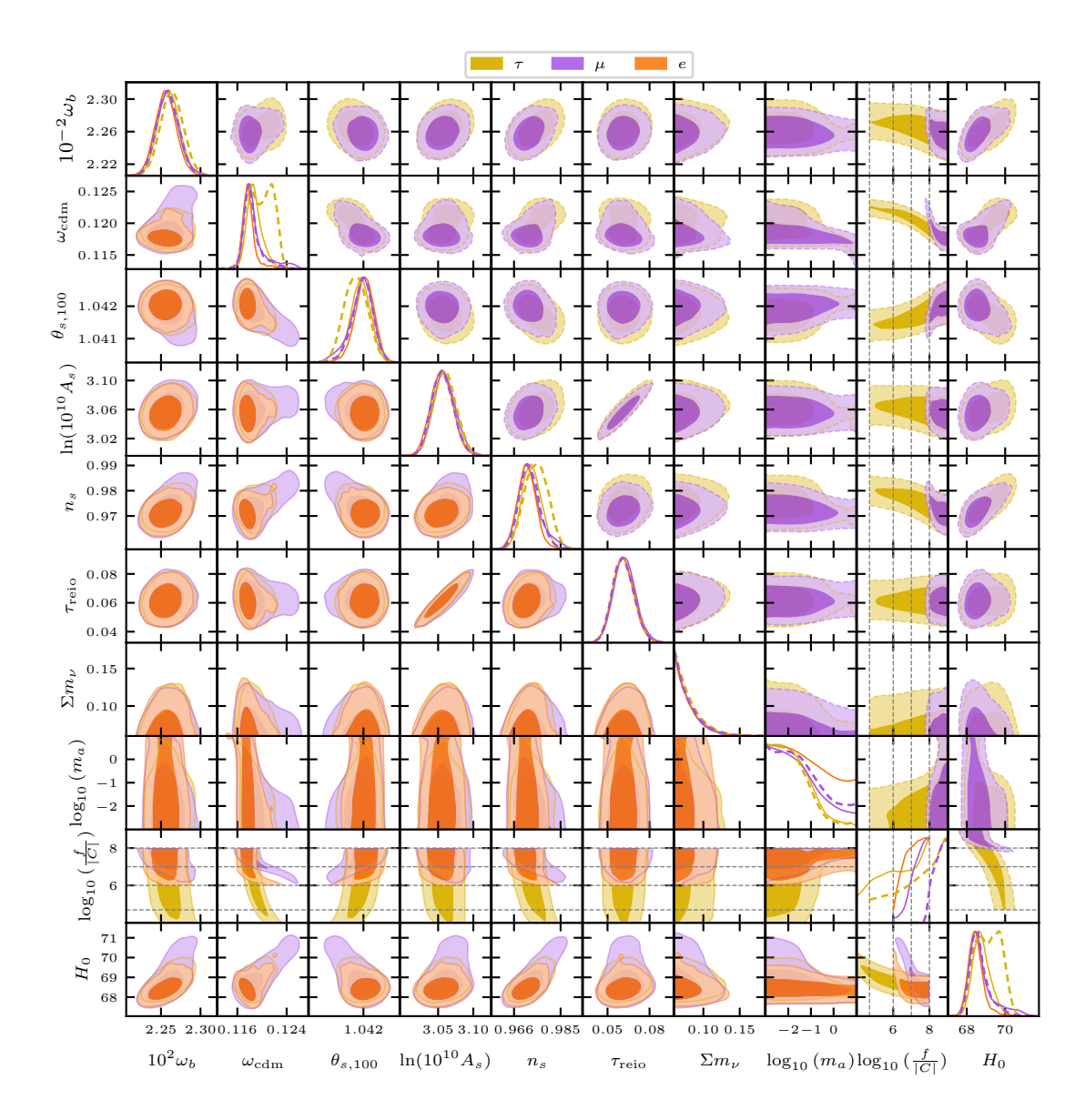


Figure 8: 1D and 2D posterior plots for all the cosmological parameters and axion parameters considered in this work and corresponding to the scans with m_a being a free parameter. The lower left half of the figure corresponds to the LFC couplings (solid lines on 1D plots), while the upper right half – to the LFV ones (dashed lines on 1D plots). Darker and lighter color shadings indicate 1σ and 2σ regions respectively. The dashed lines in the plots involving $\log_{10}(f/|C|)$ denote the boundaries on the corresponding prior used in the scans. The units of m_a and Σm_{ν} are eV, the unit of f is GeV, while H_0 is written in units of (km/s-Mpc).

with $T_0 = 2.7255$ K being the present-day CMB temperature [79]. For our demonstration we take models with axion masses $m_a = \{0.1, 1, 10\}$ eV and various values of $f/|C_{\tau l}|$ ranging from 10^5 GeV to 10^9 GeV and calculate the observables using CLASS. All other cosmological parameters in these cases are set to their maximum-likelihood values derived from our MCMC scans. These predictions are compared to the data: for D_{ℓ}^{TT} and $D_{\ell}^{\phi\phi}$ we show the Planck 2018 data [56, 57], while for P(k) we show points derived for Λ CDM from the SDSS DR7 LRG data [80, 81]. Note that in the latter case the data that we use for the demonstration is not the same as the one we use for our scans (DESI DR2), because the matter power spectrum values in case of this dataset have to be derived with some additional assumptions and the older SDSS data is sufficient for our purpose to give an idea of the scale of deviation from the standard cosmology.

In Fig. 9 we show ΔD_{ℓ}^{TT} and $\Delta D_{\ell}^{\phi\phi}$ predictions for different $f/|C_{\tau l}|$ modes from our scans and for the three aforementioned values of the axion mass. In case of $m_a = 0.1$ eV all the lines corresponding to the values of $f/|C_{\tau l}|$ shown in the legend are present, whereas for $m_a = 1$ and 10 eV only the three and two highest values appear respectively. This is because the lower values of $f/|C_{\tau l}|$ cannot provide a satisfactory fit of the cosmological data used in our scan at higher axion masses, hence these scenarios are excluded. In Fig. 10 we plot the same setup for $\Delta P(k)$. In both Fig. 9 and Fig. 10 we highlight the curves corresponding to $f/|C_{\tau l}| = 10^8$ GeV with a black outline to trace how the constraints change with mass for a given coupling value. Comparing the two figures we can see that in the considered range of masses the constraints are mainly determined by the deviation in the matter power spectrum, especially at higher masses. The evolution of the predictions for our benchmark value of the coupling with the change of mass aligns with the evolution of the constraint in Fig. 3 and supports our explanation in the main text.

References

- R.D. Peccei and H.R. Quinn, CP Conservation in the Presence of Instantons, Phys. Rev. Lett. 38 (1977) 1440.
- [2] J. Preskill, M.B. Wise and F. Wilczek, Cosmology of the Invisible Axion, Phys. Lett. B 120 (1983) 127.
- [3] L.F. Abbott and P. Sikivie, A Cosmological Bound on the Invisible Axion, Phys. Lett. B 120 (1983) 133.
- [4] M. Dine and W. Fischler, The Not So Harmless Axion, Phys. Lett. B 120 (1983) 137.
- [5] R.T. Co and K. Harigaya, Axiogenesis, Phys. Rev. Lett. 124 (2020) 111602 [1910.02080].
- [6] G. Grilli di Cortona, E. Hardy, J. Pardo Vega and G. Villadoro, The QCD axion, precisely, JHEP 01 (2016) 034 [1511.02867].
- [7] J.E. Kim, Weak Interaction Singlet and Strong CP Invariance, Phys. Rev. Lett. 43 (1979) 103.
- [8] M.A. Shifman, A.I. Vainshtein and V.I. Zakharov, Can Confinement Ensure Natural CP Invariance of Strong Interactions?, Nucl. Phys. B 166 (1980) 493.

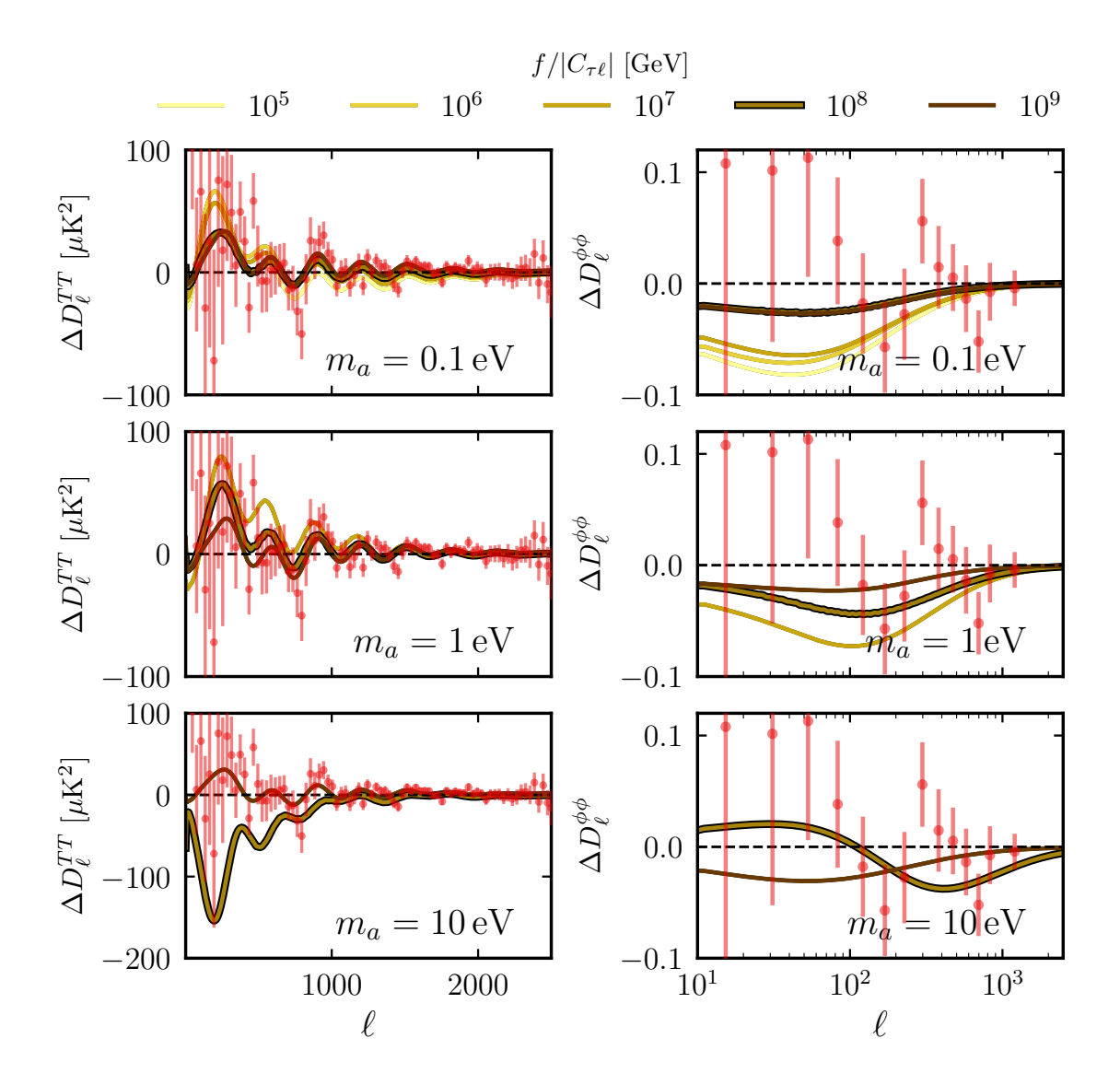


Figure 9: Differences in the CMB temperature power spectrum (left) and CMB lensing power spectrum (right) between the standard Λ CDM cosmology and scenarios with axion production via LFV τ couplings shown for axion masses $m_a = 0.1$, 1, 10 eV (from top to bottom). Each panel includes several representative values of $f/|C_{\tau l}|$ consistent with our parameter scans (cf. with Fig. 3). Note that as the mass increases, fewer values of $f/|C_{\tau l}|$ are allowed. For the sake of comparison, the case $f/|C_{\tau l}| = 10^8$ GeV is highlighted on all panels. Planck 2018 data points are overlaid for reference.

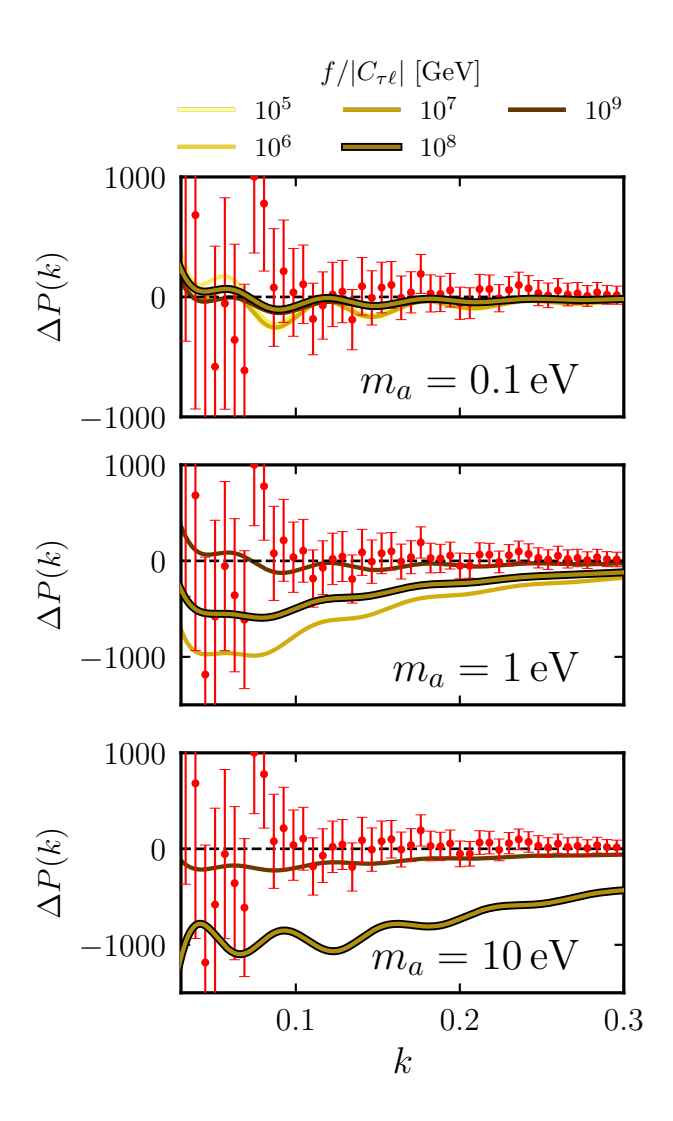


Figure 10: Differences in the matter power spectrum between the standard Λ CDM cosmology and scenarios with axion production via LFV τ couplings: $\Delta P(k) \equiv P(f/|C_{\tau l}|, k) - P_{\Lambda \text{CDM}}(k)$ shown for axion masses $m_a = 0.1$, 1, 10 eV. Each panel includes several representative values of $f/|C_{\tau l}|$ consistent with our parameter scans (cf. with Fig. 3); for the sake of comparison, the case $f/|C_{\tau l}| = 10^8$ GeV is highlighted. SDSS DR7 data points are overlaid for reference and we focus on the k values probed by it.

- [9] M. Dine, W. Fischler and M. Srednicki, A Simple Solution to the Strong CP Problem with a Harmless Axion, Phys. Lett. B 104 (1981) 199.
- [10] A.R. Zhitnitsky, On Possible Suppression of the Axion Hadron Interactions. (In Russian), Sov. J. Nucl. Phys. 31 (1980) 260.
- [11] M. Buschmann, C. Dessert, J.W. Foster, A.J. Long and B.R. Safdi, Upper Limit on the QCD Axion Mass from Isolated Neutron Star Cooling, Phys. Rev. Lett. 128 (2022) 091102 [2111.09892].
- [12] P. Carenza, B. Fore, M. Giannotti, A. Mirizzi and S. Reddy, Enhanced Supernova Axion

- Emission and its Implications, Phys. Rev. Lett. 126 (2021) 071102 [2010.02943].
- [13] L. Di Luzio, F. Mescia, E. Nardi, P. Panci and R. Ziegler, Astrophobic Axions, Phys. Rev. Lett. 120 (2018) 261803 [1712.04940].
- [14] F. Björkeroth, L. Di Luzio, F. Mescia, E. Nardi, P. Panci and R. Ziegler, Axion-electron decoupling in nucleophobic axion models, Phys. Rev. D 101 (2020) 035027 [1907.06575].
- [15] M. Badziak, G. Grilli di Cortona, M. Tabet and R. Ziegler, Flavor-violating Higgs decays and stellar cooling anomalies in axion models, JHEP 10 (2021) 181 [2107.09708].
- [16] L. Di Luzio, F. Mescia, E. Nardi and S. Okawa, Renormalization group effects in astrophobic axion models, Phys. Rev. D 106 (2022) 055016 [2205.15326].
- [17] F. Takahashi and W. Yin, Hadrophobic axion from a GUT, Phys. Rev. D 109 (2024) 035024 [2301.10757].
- [18] M. Badziak and K. Harigaya, Naturally astrophobic QCD axion, JHEP 06 (2023) 014 [2301.09647].
- [19] M. Badziak, K. Harigaya, M. Łukawski and R. Ziegler, Thermal production of astrophobic axions, JHEP 09 (2024) 136 [2403.05621].
- [20] R.T. Co, L.J. Hall and K. Harigaya, Axion Kinetic Misalignment Mechanism, Phys. Rev. Lett. 124 (2020) 251802 [1910.14152].
- [21] A. Vilenkin and A.E. Everett, Cosmic Strings and Domain Walls in Models with Goldstone and PseudoGoldstone Bosons, Phys. Rev. Lett. 48 (1982) 1867.
- [22] M. Kawasaki, K. Saikawa and T. Sekiguchi, Axion dark matter from topological defects, Phys. Rev. D 91 (2015) 065014 [1412.0789].
- [23] M. Buschmann, J.W. Foster and B.R. Safdi, Early-Universe Simulations of the Cosmological Axion, Phys. Rev. Lett. 124 (2020) 161103 [1906.00967].
- [24] M. Gorghetto, E. Hardy and G. Villadoro, More axions from strings, SciPost Phys. 10 (2021) 050 [2007.04990].
- [25] P. Panci, D. Redigolo, T. Schwetz and R. Ziegler, Axion dark matter from lepton flavor-violating decays, Phys. Lett. B 841 (2023) 137919 [2209.03371].
- [26] M. Aghaie, G. Armando, A. Conaci, A. Dondarini, P. Matak, P. Panci et al., Axion dark matter from heavy quarks, Phys. Lett. B 856 (2024) 138923 [2404.12199].
- [27] F. D'Eramo, A. Lenoci and A. Dekker, Dark Matter Freeze-In and Small-Scale Observables: Novel Mass Bounds and Viable Particle Candidates, 2506.13864.
- [28] A. Boyarsky, J. Lesgourgues, O. Ruchayskiy and M. Viel, *Lyman-alpha constraints on warm and on warm-plus-cold dark matter models*, *JCAP* **05** (2009) 012 [0812.0010].
- [29] A. Kamada and K. Yanagi, Constraining FIMP from the structure formation of the Universe: analytic mapping from m_{WDM} , JCAP 11 (2019) 029 [1907.04558].
- [30] G. Ballesteros, M.A.G. Garcia and M. Pierre, How warm are non-thermal relics? Lyman-α bounds on out-of-equilibrium dark matter, JCAP 03 (2021) 101 [2011.13458].
- [31] F. D'Eramo and A. Lenoci, Lower mass bounds on FIMP dark matter produced via freeze-in, JCAP 10 (2021) 045 [2012.01446].
- [32] Q. Decant, J. Heisig, D.C. Hooper and L. Lopez-Honorez, Lyman-α constraints on freeze-in and superWIMPs, JCAP 03 (2022) 041 [2111.09321].

- [33] Planck collaboration, *Planck 2018 results. VI. Cosmological parameters*, *Astron. Astrophys.* **641** (2020) A6 [1807.06209].
- [34] S. Chang and K. Choi, *Hadronic axion window and the big bang nucleosynthesis*, *Phys. Lett.* B 316 (1993) 51 [hep-ph/9306216].
- [35] S. Hannestad, A. Mirizzi and G. Raffelt, New cosmological mass limit on thermal relic axions, JCAP 07 (2005) 002 [hep-ph/0504059].
- [36] A. Salvio, A. Strumia and W. Xue, Thermal axion production, JCAP 01 (2014) 011 [1310.6982].
- [37] R.Z. Ferreira and A. Notari, Observable Windows for the QCD Axion Through the Number of Relativistic Species, Phys. Rev. Lett. 120 (2018) 191301 [1801.06090].
- [38] F. D'Eramo, R.Z. Ferreira, A. Notari and J.L. Bernal, Hot Axions and the H₀ tension, JCAP 11 (2018) 014 [1808.07430].
- [39] F. Arias-Aragón, F. D'Eramo, R.Z. Ferreira, L. Merlo and A. Notari, Production of Thermal Axions across the Electro Weak Phase Transition, JCAP 03 (2021) 090 [2012.04736].
- [40] R.Z. Ferreira, A. Notari and F. Rompineve, *Dine-Fischler-Srednicki-Zhitnitsky axion in the CMB*, *Phys. Rev. D* **103** (2021) 063524 [2012.06566].
- [41] D. Ghosh and D. Sachdeva, Constraints on Axion-Lepton coupling from Big Bang Nucleosynthesis, JCAP 10 (2020) 060 [2007.01873].
- [42] D. Green, Y. Guo and B. Wallisch, Cosmological implications of axion-matter couplings, JCAP 02 (2022) 019 [2109.12088].
- [43] F. D'Eramo and S. Yun, Flavor violating axions in the early Universe, Phys. Rev. D 105 (2022) 075002 [2111.12108].
- [44] F. D'Eramo, F. Hajkarim and S. Yun, Thermal Axion Production at Low Temperatures: A Smooth Treatment of the QCD Phase Transition, Phys. Rev. Lett. 128 (2022) 152001 [2108.04259].
- [45] F. D'Eramo, F. Hajkarim and S. Yun, Thermal QCD Axions across Thresholds, JHEP 10 (2021) 224 [2108.05371].
- [46] K. Langhoff, N.J. Outmezguine and N.L. Rodd, Irreducible Axion Background, Phys. Rev. Lett. 129 (2022) 241101 [2209.06216].
- [47] A. Notari, F. Rompineve and G. Villadoro, Improved Hot Dark Matter Bound on the QCD Axion, Phys. Rev. Lett. 131 (2023) 011004 [2211.03799].
- [48] F. Bianchini, G.G. di Cortona and M. Valli, QCD axion: Some like it hot, Phys. Rev. D 110 (2024) 123527 [2310.08169].
- [49] D.I. Dunsky, L.J. Hall and K. Harigaya, Dark Radiation Constraints on Heavy QCD Axions, JHEP 04 (2024) 130 [2205.11540].
- [50] K. Bouzoud and J. Ghiglieri, Thermal axion production at hard and soft momenta, JHEP 01 (2025) 163 [2404.06113].
- [51] M. Badziak and M. Laletin, Precise predictions for the QCD axion contribution to dark radiation with full phase-space evolution, JHEP 02 (2025) 108 [2410.18186].
- [52] F. D'Eramo and A. Lenoci, Back to the phase space: Thermal axion dark radiation via couplings to standard model fermions, Phys. Rev. D 110 (2024) 116028 [2410.21253].

- [53] Simons Observatory: Science goals and forecasts, JCAP 02 (2019) 056 [1808.07445].
- [54] F. D'Eramo, E. Di Valentino, W. Giarè, F. Hajkarim, A. Melchiorri, O. Mena et al., Cosmological bound on the QCD axion mass, redux, JCAP 09 (2022) 022 [2205.07849].
- [55] L. Caloni, M. Gerbino, M. Lattanzi and L. Visinelli, Novel cosmological bounds on thermally-produced axion-like particles, JCAP **09** (2022) 021 [2205.01637].
- [56] Planck collaboration, Planck 2018 results. V. CMB power spectra and likelihoods, Astron. Astrophys. 641 (2020) A5 [1907.12875].
- [57] Planck collaboration, Planck 2018 results. VIII. Gravitational lensing, Astron. Astrophys.641 (2020) A8 [1807.06210].
- [58] DESI collaboration, DESI DR2 results. II. Measurements of baryon acoustic oscillations and cosmological constraints, Phys. Rev. D 112 (2025) 083515 [2503.14738].
- [59] L.J. Hall, K. Jedamzik, J. March-Russell and S.M. West, Freeze-In Production of FIMP Dark Matter, JHEP 03 (2010) 080 [0911.1120].
- [60] P.F. De Salas, S. Gariazzo, O. Mena, C.A. Ternes and M. Tórtola, Neutrino Mass Ordering from Oscillations and Beyond: 2018 Status and Future Prospects, Front. Astron. Space Sci. 5 (2018) 36 [1806.11051].
- [61] D. Blas, J. Lesgourgues and T. Tram, The Cosmic Linear Anisotropy Solving System (CLASS) II: Approximation schemes, JCAP 07 (2011) 034 [1104.2933].
- [62] J. Lesgourgues and T. Tram, The Cosmic Linear Anisotropy Solving System (CLASS) IV: efficient implementation of non-cold relics, JCAP 09 (2011) 032 [1104.2935].
- [63] R. Takahashi, M. Sato, T. Nishimichi, A. Taruya and M. Oguri, Revising the Halofit Model for the Nonlinear Matter Power Spectrum, Astrophys. J. 761 (2012) 152 [1208.2701].
- [64] Y. Ali-Haimoud and S. Bird, An efficient implementation of massive neutrinos in non-linear structure formation simulations, Mon. Not. Roy. Astron. Soc. 428 (2012) 3375 [1209.0461].
- [65] B. Audren, J. Lesgourgues, K. Benabed and S. Prunet, Conservative Constraints on Early Cosmology: an illustration of the Monte Python cosmological parameter inference code, JCAP 1302 (2013) 001 [1210.7183].
- [66] T. Brinckmann and J. Lesgourgues, MontePython 3: boosted MCMC sampler and other features, 1804.07261.
- [67] A. Lewis, GetDist: a Python package for analysing Monte Carlo samples, 1910.13970.
- [68] I.J. Allali, A. Notari and F. Rompineve, Reduced Hubble tension in dark radiation models after DESI 2024, JCAP 03 (2025) 023 [2404.15220].
- [69] M.M. Miller Bertolami, B.E. Melendez, L.G. Althaus and J. Isern, Revisiting the axion bounds from the Galactic white dwarf luminosity function, JCAP 10 (2014) 069 [1406.7712].
- [70] A. Caputo, G. Raffelt and E. Vitagliano, Muonic boson limits: Supernova redux, Phys. Rev. D 105 (2022) 035022 [2109.03244].
- [71] Belle-II collaboration, Search for Lepton-Flavor-Violating τ Decays to a Lepton and an Invisible Boson at Belle II, Phys. Rev. Lett. 130 (2023) 181803 [2212.03634].
- [72] A. Jodidio, B. Balke, J. Carr, G. Gidal, K.A. Shinsky, H.M. Steiner et al., Search for right-handed currents in muon decay, Phys. Rev. D 34 (1986) 1967.

- [73] TWIST collaboration, Search for two body muon decay signals, Phys. Rev. D 91 (2015) 052020 [1409.0638].
- [74] L. Calibbi, D. Redigolo, R. Ziegler and J. Zupan, Looking forward to lepton-flavor-violating ALPs, JHEP 09 (2021) 173 [2006.04795].
- [75] W.L. Xu, J.B. Muñoz and C. Dvorkin, Cosmological constraints on light but massive relics, Phys. Rev. D 105 (2022) 095029 [2107.09664].
- [76] C. Heymans et al., CFHTLenS tomographic weak lensing cosmological parameter constraints: Mitigating the impact of intrinsic galaxy alignments, Mon. Not. Roy. Astron. Soc. 432 (2013) 2433 [1303.1808].
- [77] O. Garcia-Gallego, V. Iršič, M.G. Haehnelt, M. Viel and J.S. Bolton, Constraining mixed dark matter models with high-redshift Lyman-alpha forest data, Phys. Rev. D 112 (2025) 043502 [2504.06367].
- [78] J. Baur, N. Palanque-Delabrouille, C. Yeche, A. Boyarsky, O. Ruchayskiy, É. Armengaud et al., Constraints from Ly-α forests on non-thermal dark matter including resonantly-produced sterile neutrinos, JCAP 12 (2017) 013 [1706.03118].
- [79] Particle Data Group collaboration, Review of particle physics, Phys. Rev. D 110 (2024) 030001.
- [80] SDSS collaboration, The Seventh Data Release of the Sloan Digital Sky Survey, Astrophys. J. Suppl. 182 (2009) 543 [0812.0649].
- [81] S. Chabanier, M. Millea and N. Palanque-Delabrouille, Matter power spectrum: from ly-α forest to cmb scales, Monthly Notices of the Royal Astronomical Society 489 (2019) 2247.